Journal of Structural Geology 31 (2009) 1100–1113

Contents lists available at ScienceDirect

Journal of Structural Geology

journal homepage: www.elsevier.com/locate/jsg

Fracture initiation, development, and reactivation in folded sedimentary rocks at Raplee Ridge, UT

Ian Mynatt, Solomon Seyum*, David D. Pollard

Department of Geological and Environmental Sciences, Stanford University, Stanford, CA 94305, USA

ARTICLE INFO

Article history:
Received 16 April 2008
Received in revised form
30 May 2009
Accepted 2 June 2009
Available online 13 June 2009

Keywords:
Raplee Ridge
Monocline
Fracturing
Fracture sets
Fracture chronology

ABSTRACT

Fractures at Raplee Ridge, a 14 km long monoclinal fold of Pennsylvanian sedimentary rock in southeast Utah, are examined to determine their sequential development and to explain the mechanical relationships among the three primary fracture sets and the fold. Folding is attributed to slip on an unexposed thrust fault of Laramide age. Fracture orientations were measured at 98 sites and fracture patterns were mapped at 8 sites on two sandstone and two limestone units of the Rico Formation, revealing at least four stages of fracture formation. Stages 1 and 2 occurred pre-folding and are defined, respectively, by E–W trending fracture Set I and N–S trending fracture Set II. Set I fractures are characterized by a unimodal distribution of attitudes, an intermediately-developed outcrop pattern, and continuous, linear traces on bedding surfaces. Set II fractures have a greater dispersion of orientations and are poorly-to intermediately-developed. Abutting relationships confirm that Set I fractures are older than Set II. Stage 3 occurred during folding when NW–SE trending Set III fractures initiated both from isolated flaws and as wing-cracks due to right-lateral shearing along reactivated Set I fractures. Set III fractures increase in density as the fore-limb dip increases from 10° to 30°. Later stages of deformation are characterized by the formation of fracture Subsets IV and V, structurally associated with fore-limb dips greater than 30°. Fracture Sets I and II are found throughout the surrounding Monument Upwarp and are attributed to that structure, whereas Set III is attributed to local stresses induced by monoclinal folding and/or thrust faulting.

1. Introduction

Anticlinal folds often form traps for hydrocarbons (Hennings et al., 2000), and this trapping potential can be influenced by fractures that function as conduits (National Research Council, 1996; Coward et al., 1998; Haneberg et al., 1999) to channel fluids into a reservoir (Aydin, 2000) or as pathways to disperse accumulated fluids out of a reservoir (Smith, 1966; Jones et al., 1998). For these reasons, understanding the association between folds and fractures has important applications in hydrocarbon exploration and extraction.

The widespread occurrence of fractures in folded sedimentary rocks has motivated researchers to propose physical relationships between fractures and stress distributions associated with the folding process (e.g. Gilbert, 1882; Murray, 1968; Cosgrove, 2000). The findings of some recent studies (e.g. Engelder et al., 1997; Hennings et al., 2000; Bergbauer and Pollard, 2004; Bellahsen et al., 2006; Gross and Eyal, 2007; Olson, 2007) indicate complicated relationships involving the remote tectonic stress and both spatial and temporal variations in the local folding- or faulting-induced stresses, and suggest that pre-existing fractures may influence new fracture formation. These findings are at odds with older conceptual models (e.g. Price, 1966, Fig. 43; Kelley, 1987, Fig. 4) that suggest relatively simple geometric relationships between structural location on a fold and fracture orientation. They also are at odds with conceptual models (e.g. Stearns, 1969, Figs. 7 and 10; Cosgrove and Ameen, 2000, Figs. 7f,g,h and 8a) relating a locally homogeneous stress state that varies with position on a fold to the orientation and mode of fracturing, based on inferences from rock mechanics experiments. Nonetheless, these older models, or modifications of them (Cooper et al., 2006), are used to explain the formation of fractures on folds (Wennberg et al., 2006).

We show that the older conceptual models are not adequate to explain fracture development in a reservoir-scale fold at Raplee Ridge. Drawing on recent studies aimed at establishing physical relationships between fractures and folds, we characterize fractures using their orientation and position on the fold, and consider, for example, abutting relationships to determine relative ages of the

* Corresponding author.
E-mail address: solomons@stanford.edu (S. Seyum).

0191-8141/$ – see front matter © 2009 Elsevier Ltd. All rights reserved.
doi:10.1016/j.jsg.2009.06.003

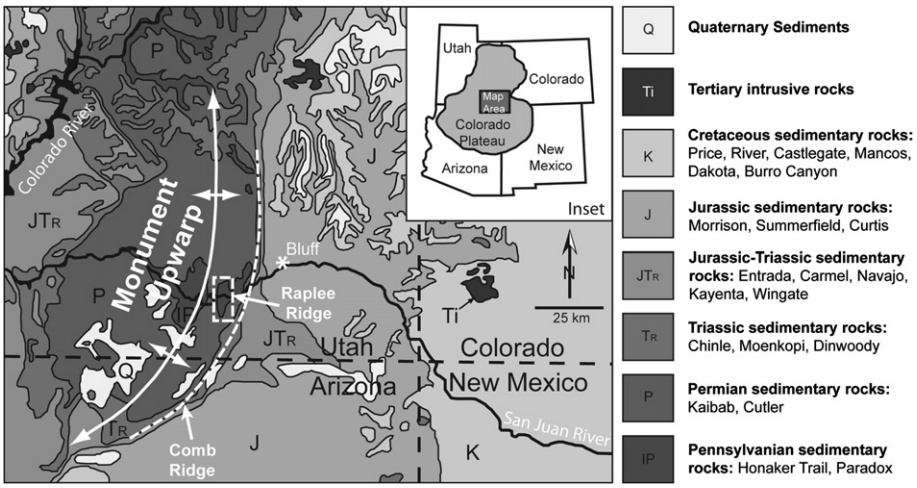

Fig. 1. A geologic map of southeastern Utah displaying the geographic locations of Monument Upwarp, Raplee Ridge and Comb Ridge. Modified from map by Bump and Davis, 2003. A white dashed line traces the length of Comb Ridge. Raplee Ridge is outlined with a rectangular box.

fracture sets, their sequential development relative to the folding, the reactivation of some fractures as the stress state evolves, and the initiation of new fractures as wing cracks. The basis for these additional interpretations starts with detailed mapping and geometric measurements, but also employs mechanical concepts such as frictional sliding, stress concentrations, and fracture propagation paths.

2. Field area: Raplee Ridge, Utah

The Colorado Plateau tectonic province in the southwestern United States (Fig. 1) is known for its large, well-exposed, and visually spectacular monoclinal folds (Davis, 1978; Davis, 1999; Bump and Davis, 2003). The Monument Upwarp in southeastern Utah, is bounded along its eastern margin by one of these great monoclines, called Comb Ridge. This structure is interpreted as an example of Laramide-style deformation, usually associated with "thick-skinned" orogenic processes, during which the folds are induced by thrust faults emanating from the pre-Cambrian crystalline basement (e.g. Davis, 1978; Reches and Johnson, 1978; Stone, 1993; Huntoon, 1993; Erslev, 1993; Tindall and Davis, 1999; Bump, 2003). A smaller monocline, called Raplee Ridge (Fig. 2), is located on the Monument Upwarp, about 8 kilometers west of Comb Ridge. This field site provides exceptional opportunities to examine the geometric and chronologic relationships between this kilometer-scale fold and both pre-existing and synchronous outcrop-scale fractures.

The fold at Raplee Ridge is interpreted as forming during the Laramide Orogeny, bracketing its time of formation between the late Cretaceous period and the Eocene epoch (Gregory and Moore, 1931; Goldstrand, 1994; Bump and Davis, 2003). The fold axis trends approximately north–south and the cross-sectional form is asymmetric, with beds dipping up to 40° to the west and only about 5° to the east. As a result, the fold is described in the literature as both a monocline and an anticline (Ziony, 1966; Delaney et al., 1986; Stevenson, 2000). It is approximately 14 km long with almost 500 m of structural relief. The gently-plunging southern nose trends 175° and the gently-plunging northern nose trends 015°, giving the fold an arcuate shape in map view (O'Sullivan, 1965; Ziony, 1966).

The stratigraphic units exposed on Raplee Ridge (Fig. 3 and 4a) are of Pennsylvanian and Permian age (Cross et al., 1899; Jentgen, 1977). Of particular interest is the ~140 m thick Rico Formation, which is composed of thick, red, slope-forming shale layers separated by eight erosionally resistant and distinctive layers of sandstone and limestone (O'Sullivan, 1965; Ziony, 1966). The resistant units that crop out at Raplee Ridge display systematic joint and fracture sets both in cross section views and on pavements that expose their tops.

Previous studies on the Colorado Plateau have used the patterns of joints (e.g. Kelley and Clinton, 1960; Bergerat et al., 1992), deformation bands, and other small-scale structures (e.g. Davis, 1999; Bump and Davis, 2003) in the sedimentary rocks to interpret Laramide uplifts and associated monoclines, and to infer the geometry and kinematics of possible underlying basement faults. Rather than using outcrop-scale structures to constrain the inferred basement fault at Raplee Ridge, Mynatt et al. (2007) and Hilley et al. (in press) used the geometry of the fold itself, determined from Airborne Laser Swath Mapping (ALSM) data. They employed inverse theory and the Boundary Element Method, implemented in the computer code Poly3D (Thomas, 1993; Maerten et al., 2005; Maerten et al., 2006), to generate displacement fields associated with slip on model faults with a range of geometries. A displaced horizon in the model simulated the folded shape of the McKim

Fig. 2. Oblique, aerial photograph of the middle portion and northern end of Raplee Ridge. The upper right asterisk marks the highest point of the ridge, whereas the lower left asterisk marks the lowest point. The difference in elevation of these two points is ~370 m and the horizontal distance is ~1420 m. The point-to-point distance is ~1470 m.

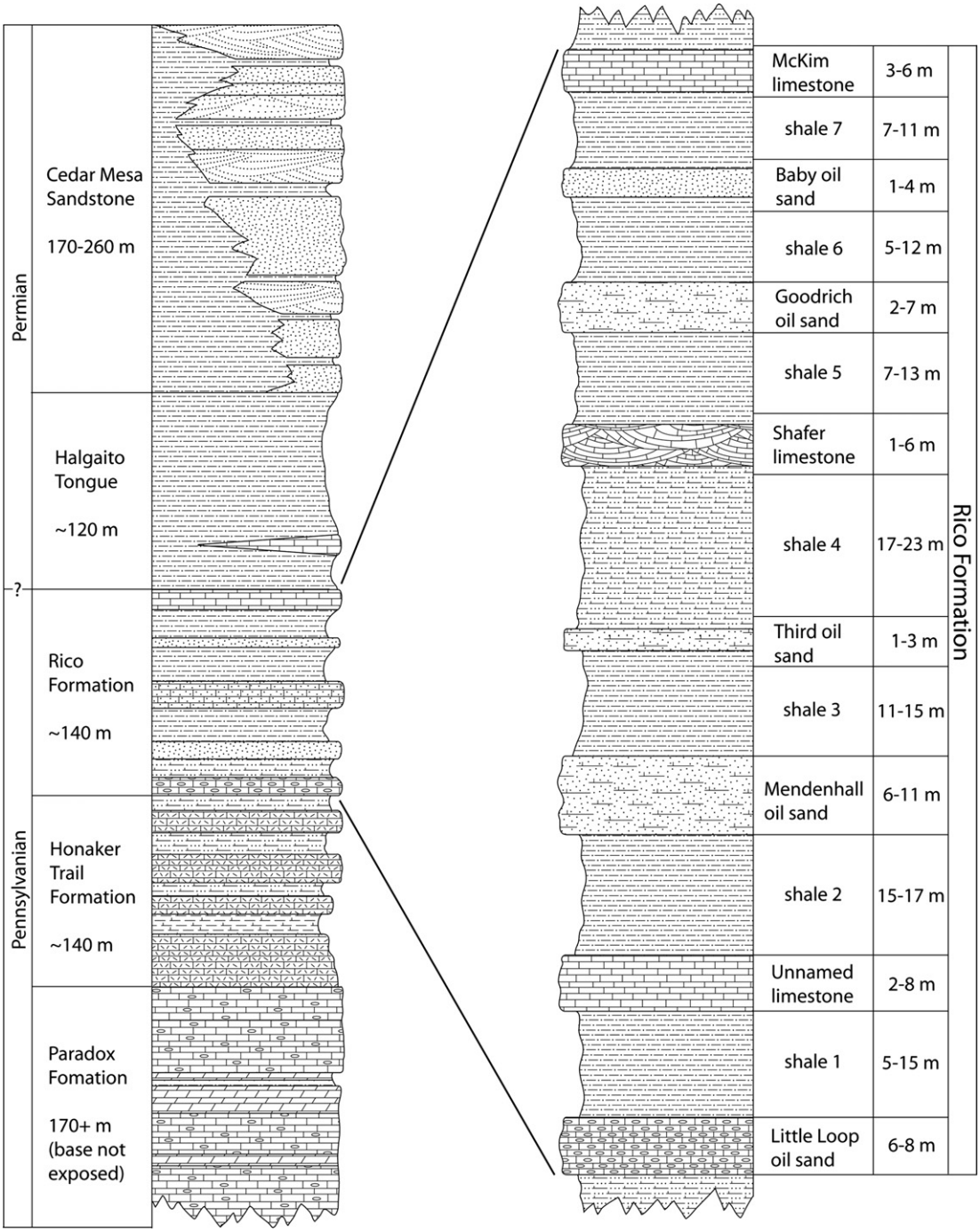

Fig. 3. The stratigraphic column of units exposed at Raplee Ridge. Fractures were measured and mapped in the Goodrich, Shafer, Mendenhall and Unnamed members of the Rico Formation. The exact location of the Pennsylvanian–Permian boundary is unknown and may lie within the Rico Formation. Modified from Ziony, 1966.

limestone at the top of the Rico Formation (Fig. 3) to constrain the fault geometry. The best-fitting fold model was associated with a reverse fault oriented 003°/44°, with 16 km in strike length, 6.6 km in down-dip length, and an upper tip 0.8 km below the current exposed surface. This suggested fault mechanism for the formation of the Raplee Ridge monocline is not directly verifiable because no underlying fault is exposed.

3. Previous Work

This study builds on earlier work done in the region by Ziony (1966), who mapped fractures at Raplee Ridge and the surrounding area, including nearby Comb Ridge and the lesser fold at Halgaito Ridge (Fig. 5). Areas on the map lacking fracture lines have poor exposure, are inaccessible, or were not visited by Ziony. He identified two regional fracture sets striking nearly E–W, and interpreted them as a conjugate pair. Ziony identified a third regional set, striking N–S, based on his determinations of relative ages. He also identified a NW–SE set, spatially associated with the major structures in the area, including Comb, Halgaito, and Raplee Ridges.

We did not find consistent field evidence at Raplee Ridge to distinguish the relative ages of Ziony's first two fracture sets; such as one set systematically abutting the other. Nor did we find sufficient diagnostic evidence, such as slickenlines and mutually

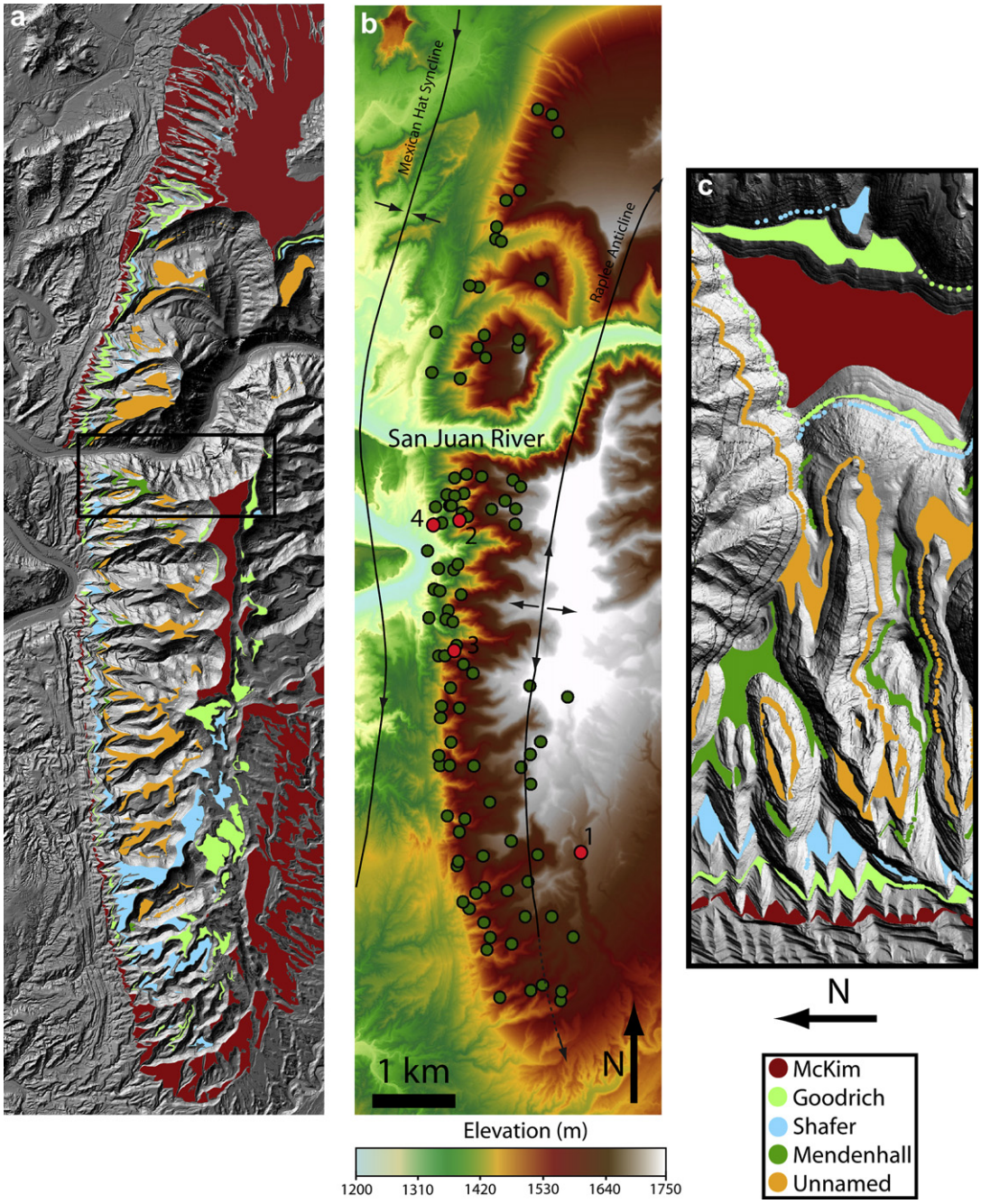

Fig. 4. a) Geologic map of stratigraphic units from the Rico Formation (Fig. 3) mapped onto a hill-shaded visualization of ALSM data. b) An elevation map of Airborne Laser Swath Mapping (ALSM) data of Raplee Ridge. Green dots show locations of 98 fracture measurement sites. Red dots are fracture map locations that have been included in this paper, with map numbers. The Mexican Hat Syncline and Raplee Anticline fold hinges have been superimposed on this image from the Photogeologic Map of the Bluff-11 Quadrangle by C.F. Miller (1955). c) Close up of area demarcated by a black rectangle in a) to show detail of mapped stratigraphic units.

offsetting relationships, to infer that these fractures formed as conjugate shear fractures. Therefore, Ziony's first two sets are relabeled Set I and are shown as E–W trending red lines on Fig. 5. We have not investigated more than a few outcrops away from Raplee Ridge, so we offer this interpretation merely as an alternate working hypothesis for the region. We note that the newly defined Set I is broadly distributed throughout the region with only minor variations in strike. Ziony's third set is relabeled Set II on Fig. 5 and is indicated by N–S trending blue lines. Set II is restricted to specific locations in the region mapped by Ziony (1966), and is not present at all the outcrops where Set I is exposed. Ziony's fourth set is relabeled Set III on Fig. 5 and is indicated by NW–SE trending green lines. With few exceptions, Set III fractures are spatially associated with the folds at Halgaito, Raplee, and Comb Ridges.

4. Field and mapping methods

Partially fracture orientations were measured at bedrock exposures along the length of the fold, and fractures were mapped and characterized in detail at a few particularly well-exposed top surfaces of erosionally resistant limestone and sandstone units. This new information serves to document the geometries and chronologies of fractures at Raplee Ridge. Attitudes of about 30 to 50 fractures were taken from each outcrop on the fold (green

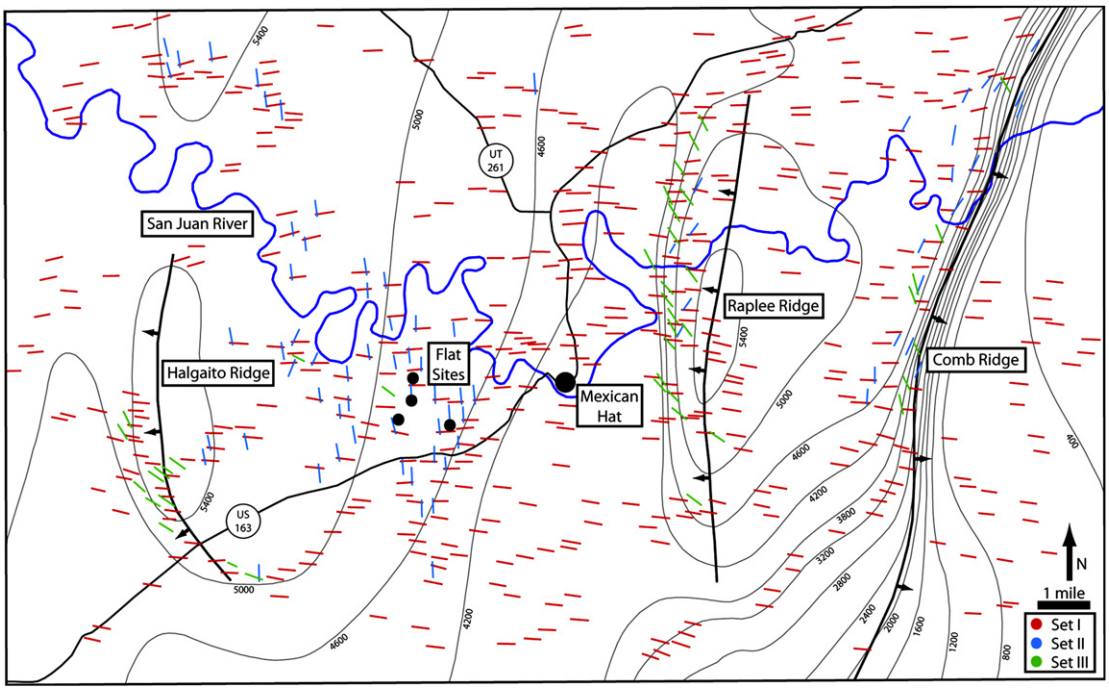

Fig. 5. A map of Set I, II, and III fractures around Raplee Ridge, UT. Structure contours are estimated for the top of the McKim limestone. Black lines with arrows are fold hinges, where the arrows are pointing toward the forelimbs. Four fracture measurement sites west of Raplee Ridge, in nearly horizontal strata, are shown as small black dots and labeled "Flat Sites." Modified from Ziony (1966).

circles, Fig. 4b) for a total of 3,697 fracture orientations. Four outcrops, from nearly horizontal surfaces to the west of the fold (black circles, Fig. 5), were also studied for comparative purposes.

Detailed fracture maps were made at eight outcrops (Mynatt, 2009), four of which are described in this paper (red circles, Fig. 4b). These locations represent similar positions in the stratigraphic section that are distributed over the fold where the structural relationships among fractures are well displayed. We used the outcrop-scale maps to identify the relative ages of fracture sets, the localized occurrence of fractures, the mode of fracture initiation (opening or shearing) for the different fracture sets, and to determine diagnostic criteria for the reactivation of pre-existing fractures.

The fracture maps were stitched together in Adobe Photoshop® using high-resolution, 12 mega-pixel photographs of exposed bedding tops to create a complete image of the outcrop. Ten to twenty points on each outcrop were surveyed using a Trimble ProXH® GPS and a Contour XLRic® laser range finder to accurately record position locations in three dimensional space. The merged photographs were orthorectified in ARCmap® using these surveyed points. The orthorectified images for each of the sites were printed in large format ($\sim 1 \times 2$ m) and the fractures were mapped on these images in the field and later digitized using Adobe Illustrator®.

The geologic map (Fig. 4a,c) of the Rico Formation was made by combining the ALSM topographic data with field mapping. Large ($\sim 1 \times 2$ m) printouts of the ALSM data served as base maps, allowing the meter-scale resolution of the data to be visualized and utilized at the outcrop. Each color on the geologic map corresponds to exposures within the upper two meters of the respective units in order to constrain the locations of unit tops for use in geometric modeling (e.g. Mynatt et al., 2007; Hilley et al., in press). Unit tops were identified in the field and mapped onto the ALSM base maps. The five mapped members of the Rico Formation (Fig. 3) crop out both as broad pavements and as narrow ledges protruding from larger slope faces. All location data was digitized using ARCmap®, with the pavements outlined as polygons and the ledges demarcated by a series of points (Fig. 4c).

5. Overview of fracture-fold chronology

Partially following the definition of Hodgson (1961), systematic fracture sets are composed of approximately planar fractures that are nearly perpendicular to bedding, occur at similar orientations across a significant area, and locally cut across other fractures. We define subsets as fractures that occur at multiple locations, and have similar orientations at all locations, but are more sporadic and limited in areal extent. Fractures of a given set or subset are assumed to have formed under similar loading conditions that result in particular initiation and propagation mechanisms (Pollard and Aydin, 1988). Each of these unique loading states leading to fracture formation is defined as a deformational stage, and we identify and describe four at Raplee Ridge. To determine the relative age of fracture sets, the statistics of the fracture abutting relationships were compiled for each fracture map.

The fracture sets do not bear any systematic relationship to topography, as would be expected if they formed at or near Earth's surface. Fractures that are sub-parallel in strike to nearby, steep topographic slopes are a common feature at Raplee Ridge, but only where the topographic slope happens to coincide in strike with one of the identified fracture sets. Furthermore, the fracture sets have consistent strikes relative to geographic coordinates throughout the area (Fig. 5), and are therefore found in all possible geometries with respect to topographic slopes. All three sets occur stratigraphically throughout the Rico Formation, which is ~100 m thick. Set I also is stratigraphically continuous throughout the exposed 840 m of section. In summary, the lack of a geometric correlation to topographic features, the consistent orientation of the fracture sets across the region, and the stratigraphic continuity of Set I are used to infer that the fractures formed in the subsurface and not at the ground surface.

We differentiate three major systematic fracture sets from all sites at Raplee Ridge using the SpheriStat™ stereogram program, which are consistent with the three fracture sets identified in the field (Table 1). For comparison, fractures were rotated to show

attitudes in the unfolded strata, noting that the majority are approximately perpendicular to bedding. Plotting and contouring all 3697 orientations together shows three distinct clusters of poles to fracture planes (Fig. 6a). Set I (Fig. 6b) has a mean fracture plane orientation of 092°/90° with a spherical variance of 0.05; Set II (Fig. 6c) has a 197°/88° mean orientation and a spherical variance of 0.072; and Set III (Fig. 6d) has a mean orientation of 320°/89° and a spherical variance of 0.071. Cluster analysis using the SpheriStat™ algorithm indicates unimodal distributions, suggesting that none of the sets are composed of conjugate fractures. For example, if two trial cluster mean orientations are placed arbitrarily on the stereogram with Set I data, the data are subdivided nearly symmetrically according to the placement of the trial mean orientations, rather than being subdivided by any inherent bimodality of the population itself. Each fracture measurement site (Table 2, supplementary archive) was checked individually and no fracture set at any site had a bimodal distribution.

The fracture sets are interpreted as those that initiated under stress states that apparently pre-dated significant folding at Raplee Ridge, and those that were synchronous with the folding event. We identify two sets of pre-folding fractures, E–W striking Set I and N–S striking Set II. These set numbers are based on relative ages deduced from outcrop observations of fracture abutment relationships (Table 3), with Set I identified as being older than Set II. We identify Set III as a syn-folding fracture set striking NW–SE. Finally, we identify Subsets IV and V that appear only locally and are also interpreted as syn-folding (Mynatt, 2009).

The chronology of fracturing determined on Raplee Ridge is similar to that concluded by Ziony (1966). However, Ziony noted locations where two pre-folding fracture sets mutually abut and cross-cut, suggesting formation of both sets during a common deformation stage. The absence of conjugate fractures at outcrops that were mapped in great detail, and their absence in the statistical analysis of fracture orientation data (Fig. 6), indicate an important difference with Ziony's interpretation. Additionally, newly identified fractures, Subsets IV and V were found.

6. Pre-folding fractures

In qualitative terms, Set I is the most prevalent of the fracture sets across the region (Fig. 5), occurring on and between the three folds (ridges) on this part of the Monument Upwarp. This set is present at all mapped sites and in all stratigraphic units exposed at Raplee Ridge (Fig. 3). Both Ziony (1966) and Delaney et al. (1986) noted its "stratigraphically continuous" nature, documenting that Set I fractures cut through multiple units and are present throughout the exposed stratigraphic column (Fig. 3) in contrast to all other local and regional fracture sets. For example, Set II fractures are less well represented or absent in the weakly lithified, red silt and shale layers (shales 1–7) between the more erosionally resistant limestone and sandstone layers of the Rico Formation. Thus, Set I can be differentiated by its stratigraphic ubiquity from Set II.

The unfolded orientations of the three major fracture sets on Raplee Ridge are shown in Fig. 6. Set I fractures have a lesser dispersion (0.05 spherical variance) than Set II (0.072 spherical variance) or Set III (0.071 spherical variance), reflecting that Set I is more consistently oriented both locally and across Raplee Ridge (Fig. 7). Additionally, the mapping by Ziony (1966) shows that Set I orientation is more consistent than Set II or Set III throughout the region (Fig. 5).

Qualitatively, Set I fracture traces tend to be straighter and fracture surfaces tend to be more nearly planar than Set II or III fractures. On outcrop Maps 1, 2, and 3 (Figs. 8–10), Set I fracture traces are the longest and most continuous, and would be interpreted using Hodgson's criteria as the systematic set (Hodgson, 1961). The quantitative classification of fracture set spacing proposed by Wu and Pollard (1995, equation 9, Table 1) was modified to incorporate multiple sub-regions of each map. Spacing measurements were made directly on the outcrop maps for each fracture set. Area measurements were simplified by approximately outlining map boundaries with straight sides, and dividing the maps into regular polygons avoiding gaps of unmapped sections when measuring spacing between fractures along a scanline. Each polygon, or sub-region, of a map was measured individually for area, A, and spacing, S. The deviations of normalized individual spacing from the area spacing for Set I on Maps 1, 2, and 3 are 0.494, 0.464, and 0.644 respectively. In other words, Set I fractures are intermediately-developed. In contrast, the deviations for Set II are 0.575, 0.677, and 0.621 respectively, making them poorly-to intermediately-developed. For Set III on Maps 2 and 3 the deviations are 0.83 and 1.12 respectively, making them poorly-developed. We do not imply anything about fracture saturation (Bai and Pollard, 1999) here because thickness measurements of the fractured layers are lacking.

Both fracture Sets I and II appear at more than 100 sites investigated by Ziony (Fig. 5) away from the three major folds of the region. We documented these fracture sets at four sites to the west of Raplee Ridge in slightly tilted (<8° dip) to flat-lying sedimentary layers. Because abutting relations (Table 3) indicate that Sets I and II are older than fracture Set III, and Set III is found exclusively on the fold, we suggest the formation of Sets I and II pre-dates the folding event. Sites on the fold at Raplee Ridge with near-zero curvature and low bedding dip, such as Fracture Map 1 (Fig. 8) located on the backlimb of the fold where the dip is about 5°, contain only Set I and Set II fractures.

Abutting relationships, for example on Map 1 of the Goodrich sandstone with a bedding dip of ~5° (Fig. 8), overwhelmingly confirm that Set I predates Set II (Table 3). Fracture Maps 2 and 3 show the exposed top of the Unnamed limestone with dips of ~24° and ~30° respectively (Figs. 9 and 10). On Map 2, of the 55

Table 1
Mean fracture orientations and spherical variances based on individual fracture sets of all outcrop sites on Raplee Ridge. Set clusters are identified in two ways: SpheriStat™ cluster analysis and field observations.

Set	Pole to Plane			Plane		*N*	
	Mean azimuth (°)	Mean plunge (°)	Standard deviation of E	Mean strike (°)	Mean dip (°)		
Set 1	002	01	0.050	092	90	1605	Sets determined using cluster analysis
Set 2	107	02	0.072	197	88	1188	
Set 3	230	01	0.067	320	89	904	
Set 1	002	01	0.045	092	89	1600	Sets determined in the field
Set 2	106	02	0.066	196	88	1254	
Set 3	229	02	0.075	319	88	843	

Excludes fractures measured away from Raplee Ridge.
N = number of fractures measured; E = Maximum Eigenvalue; Standard deviation of E = spherical variance.
Note: If the spherical variance = 1, there is maximum dispersion of data. If the spherical variance = 0, all data points have the same orientation.

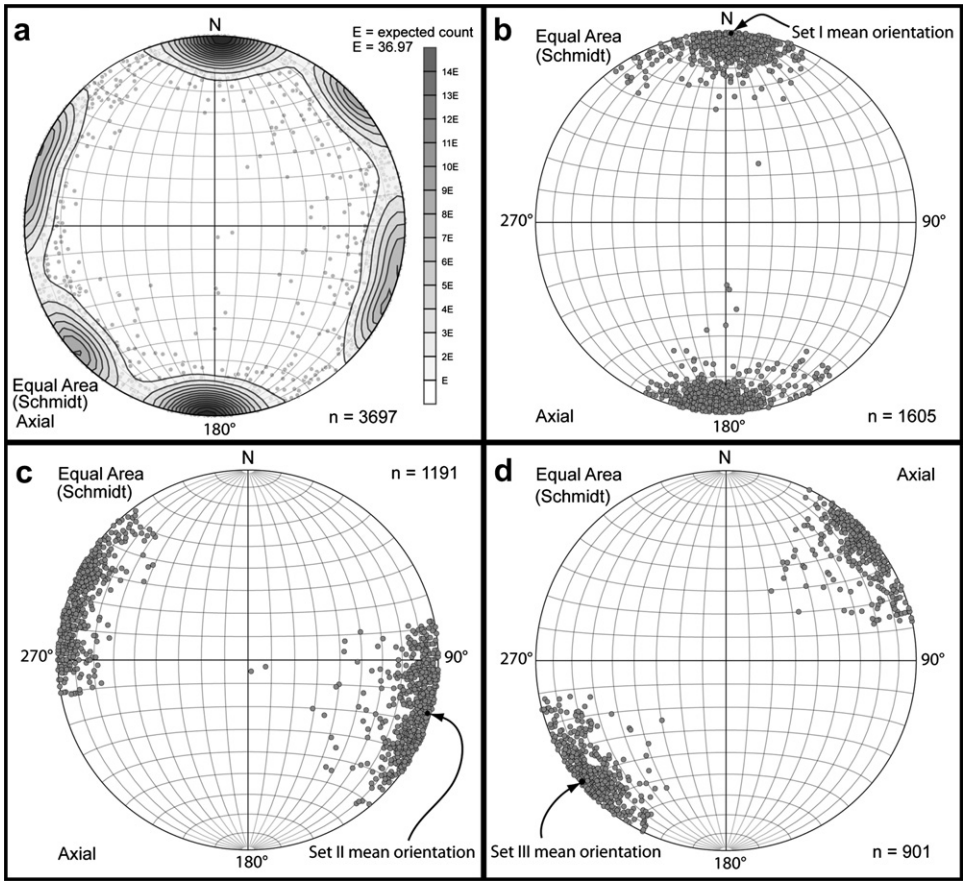

Fig. 6. Equal area stereonet plots of poles to 3697 fractures from 98 sites. SpheriStat™ v2.2 stereonet tool was used to plot Gaussian density distribution contours ($K = 100$) and to perform cluster analyses that statistically distinguish different data sets based on orientation. The cluster analysis attributes 1605 data points to Set I, 1188 points to Set II, and 904 points to Set III. a) Unfolded fracture orientations with density distribution contours. The scale bar indicates the number of points that have significant influence on an arbitrary position centered within a 1% counting circle. *E* is the expected count within the circle if the data points were evenly distributed across the net. b) Set I cluster: mean fracture plane orientation is 092°/90° with a spherical variance of 0.05. c) Set II cluster: mean fracture plane orientation is 197°/88° with a spherical variance of 0.072. d) Set III cluster: mean fracture plane orientation is 320°/89° with a spherical variance of 0.071.

Table 3
Abutment relationships between fractures measured at detailed mapping sites.

Map	Formation	Bedding dip	Abutment relationship	Number of abutments
1	Goodrich oil sand	~5°	Set I abuts Set II	1
			Set II abuts Set I	255
2	Unnamed limestone	~24°	Set I abuts Set II	1
			Set I abuts Set III	0
			Set II abuts Set I	54
			Set II abuts Set III	11
			Set III abuts Set I	42
			Set III abuts Set II	4
3	Unnamed limestone	~30°	Set I abuts Set II	12
			Set I abuts Set III	7
			Set II abuts Set I	135
			Set II abuts Set III	3
			Set III abuts Set I	36
			Set III abuts Set II	11
4	Shafer limestone	~32°	Set I abuts Set II	5
			Set I abuts Set III	7
			Set II abuts Set I	8
			Set II abuts Set III	33
			Set III abuts Set I	4
			Set III abuts Set II	5

locations where Set I and II fractures abut, there is only one example of a Set I fracture abutting against a Set II fracture (Table 3). For Map 3, Set II fractures abut against Set I fractures in 92% of the cases, further confirming the relative age interpretation for the regional fractures.

The relatively narrow strike distribution for Set I (Fig. 6b), implies a relatively uniform orientation of the horizontal principal tectonic stresses over the mapped area (Fig. 5). Interpreting the Set I fractures as opening mode (e.g. Pollard and Aydin, 1988), the least compressive principal stress, σ_3, was oriented approximately N–S during the formation of the set. Using the same interpretation, Set II formed in a regional tectonic stress field with σ_3 approximately E–W. This new stress geometry could occur either by a nearly 90° rotation in the principal stress orientations about the vertical axis, or by changes in principal stress magnitudes without rotation such that the E–W principal stress became the least compressive stress. The greater dispersion of orientations for Set II suggests a lesser difference in the magnitudes of the principal stresses (Olson and Pollard, 1989; Whitaker and Engelder, 2005), which would facilitate such a change. An alternate possibility is that the principal tectonic stresses did not rotate or change magnitudes, but the Set I joints induced a local stress rotation of about 90°, facilitating the formation of the later orthogonal set (Bai et al., 2002).

The significant differences in the geometric characteristics of Sets I and II may be related to the tectonic loading, but we suggest

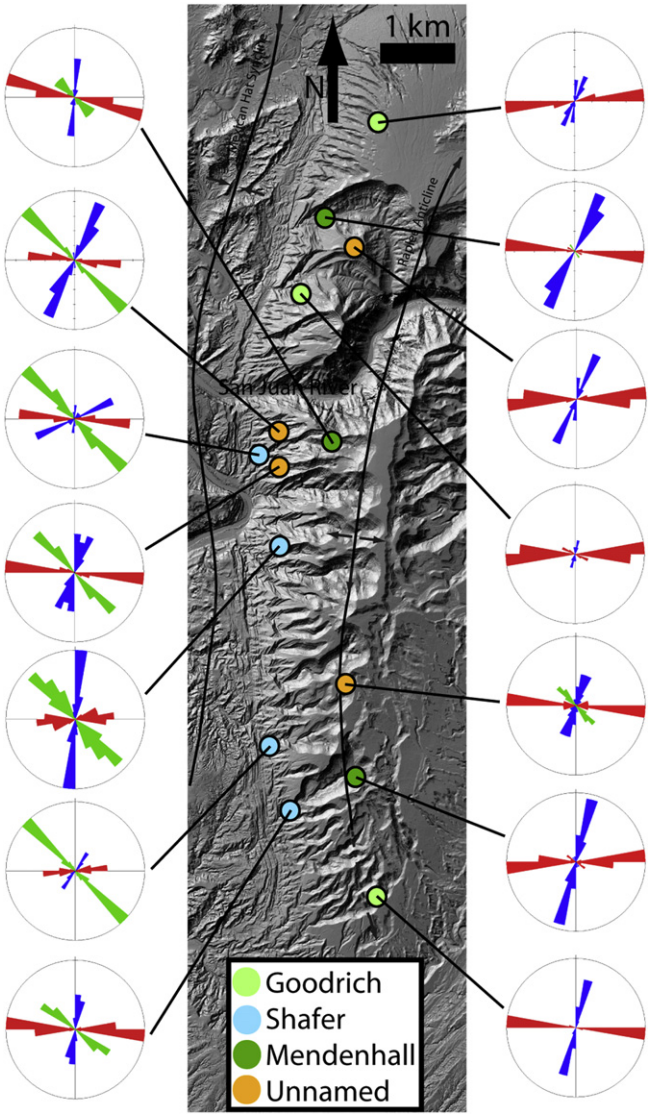

Fig. 7. Hill-shaded relief map from ALSM data of Raplee Ridge with rose diagrams of unfolded fracture strike trends from representative locations on the fold. Red = Set I, Blue = Set II, Green = Set III. Note that the variation in fracture trend of a given set between locations tends to be greater than the variation at a given location.

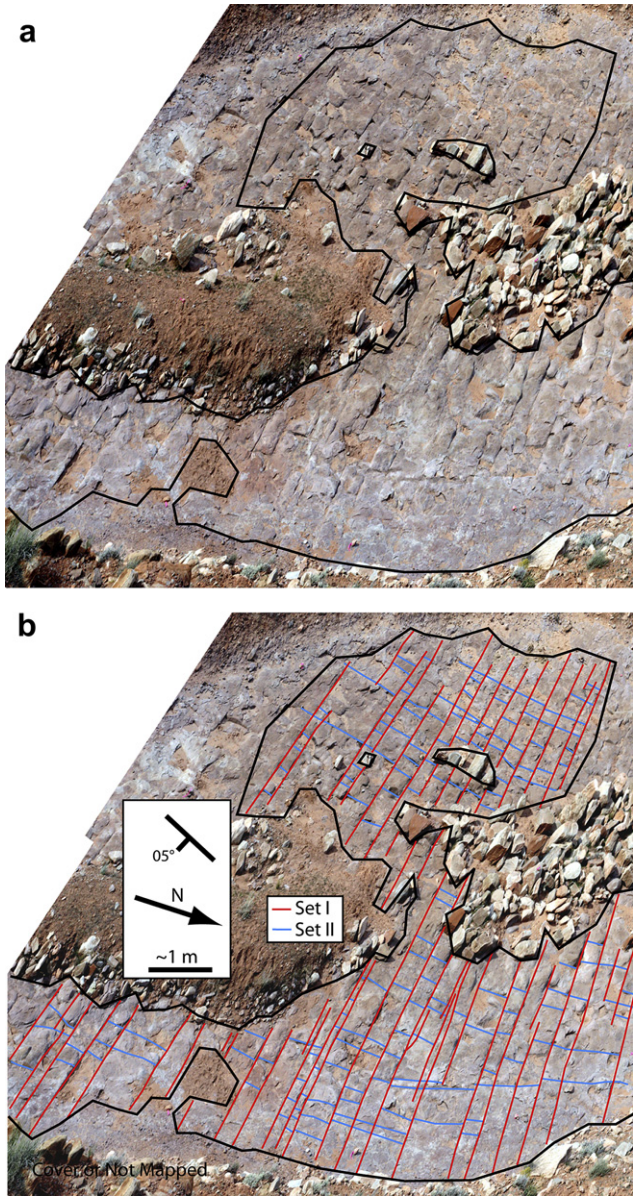

Fig. 8. Fracture Map 1 of the Goodrich sandstone. The average bedding orientation at this outcrop is ~025°/05°. a) A photograph of the outcrop with an outline of the mapped area. b) Map of Set I and Set II fractures.

that they arise at least in part due to the presence of Set I during the formation of Set II. As Set II initiated and propagated, these fractures encountered pre-existing Set I fractures. In some places, Set II fractures terminated against Set I fractures, but in other places members of Set II propagated through members of Set I. This implies that Set I fractures were tightly closed and/or sealed by secondary cementation at some localities and not at others. Cements were noted in certain members of all the fracture sets at Raplee Ridge, but the occurrence, composition, and distribution of these minerals was not investigated. Local compressive stress acting across Set I fractures could have been sufficient to hold them closed and enable cross-cutting at some localities and not at others (Renshaw and Pollard, 1995).

Another mechanical inference can be drawn from contrasts in the geometric nature of Sets I and II. Whereas Set I usually is intermediately-developed, Set II usually is poorly-to intermediately-developed, and is almost absent at some locations. This geometric difference suggests the effective tension driving Set II was less than that during the formation of Set I (Wu and Pollard, 1995). This difference in driving stress is supported by noting the stratigraphic continuity of Set I and the paucity of Set II in the more shaley layers (shales 1–7, Fig. 3): often Set II is limited in vertical extent to a single sandstone or limestone bed. Apparently the effective tensile stress was insufficient to drive the Set II fractures into the shale layers or, in many instances, across the older Set I fractures.

7. Folding-related fracture set

The systematic fracture set labeled Set III (Fig. 6d) is structurally associated with the forelimb of the fold at Raplee Ridge (Fig. 7). It is conspicuously absent from the nearly flat-lying sedimentary rocks to the west and east of Raplee Ridge (Fig. 5) and from the northern and southern noses of the fold (Figs. 5 and 7) where the fold amplitude, bedding dip, and bedding curvature are least. These observations suggest that Set III was induced by the folding. Ziony (1966) mapped similarly oriented fractures on the forelimbs of the

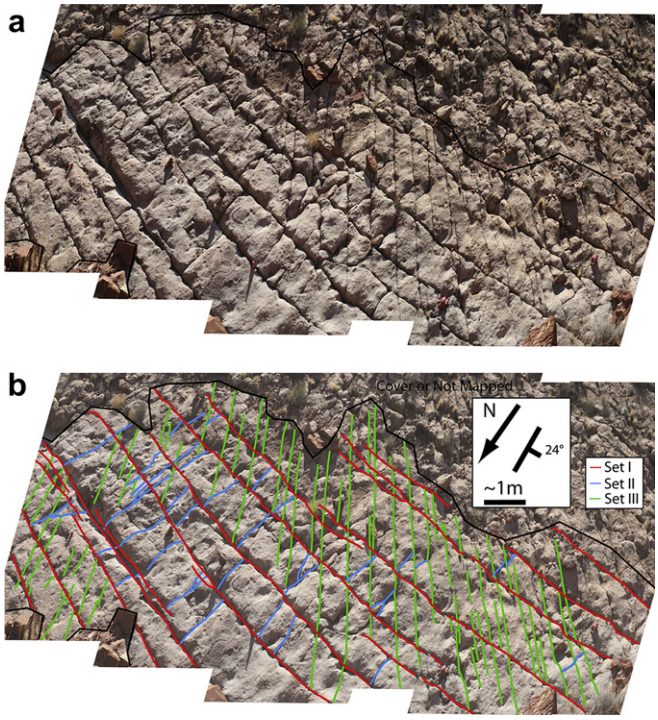

Fig. 9. Fracture Map 2 in the Unnamed limestone. The average bedding orientation at this outcrop is ~175°/24°. a) A photograph of the outcrop with an outline of the mapped area. b) Map of Set I, II, and III fractures.

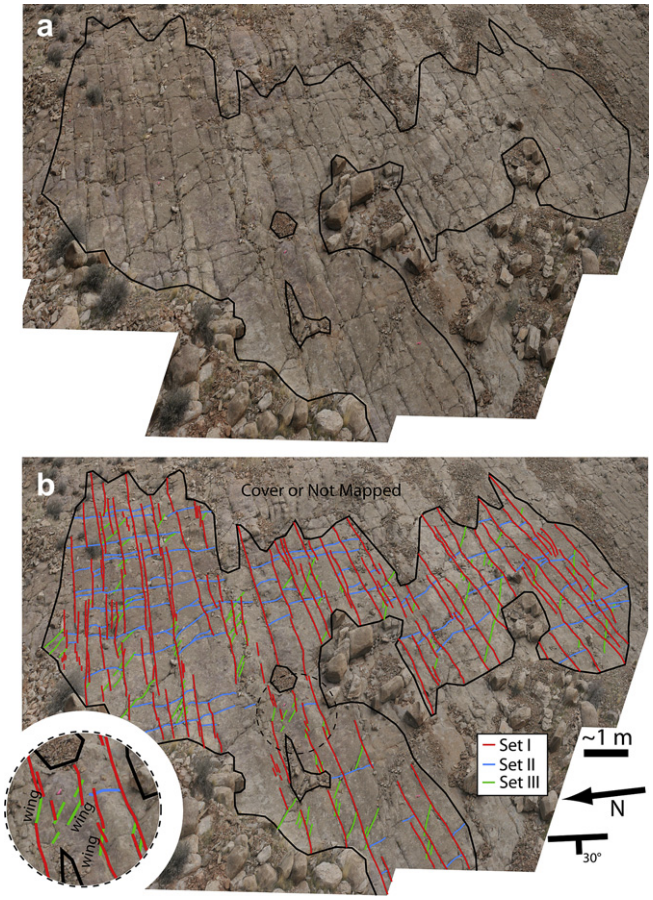

Fig. 10. Fracture Map 3 in the Unnamed limestone. The average bedding orientation at this outcrop is ~184°/30°. a) A photograph of the outcrop with an outline of the mapped area. b) Map of Set I, II, and III fractures. Lower left, circular inset is a close-up view of the map section outlined by a dashed circle displaying typical Set III wing fractures.

Raplee, Comb and Halgaito flexures (Fig. 5), implying that the fracturing histories and mechanisms may be similar for all three folds.

Two mechanisms involved in the initiation of the Set III fractures have been identified. Some Set III fractures on Map 2 (Fig. 9) appear as longer, through-going fractures whose initiation mechanism may involve grain-scale flaws (Pollard and Aydin, 1988), similar to Set I and II fractures. Other Set III fractures intersect Set I fractures in a geometry suggesting they formed as wing-cracks (Griffith, 1924; Willemse and Pollard, 1998; de Joussineau et al., 2007; Mutlu and Pollard, 2008) in response to Mode II shearing along Set I (Fig. 10). These fractures make an acute angle in the clockwise direction to Set I fractures at which they terminate. Locally identified right-lateral offset along Set I fractures is consistent with, and found in the same outcrop as Set III fractures, which are interpreted as wing-cracks. Independent evidence of right-lateral shearing along Set I is shown by offset Set II fractures (Fig. 11a), calcite slicken fibers on fractures in limestone (Fig. 11b), and en echelon calcite veins sub-parallel to Set I (Fig. 11c).

The restricted occurrence of Set III to the forelimb of the fold (Fig. 7) suggests that these fractures are related to an increase in bedding dip and/or their proximity to the underlying thrust fault. Set III fracture density has a strong positive correlation with bedding dip in both the Goodrich sandstone and Shafer limestone (Fig. 12). Relationships for Set III fractures (Table 3) show abutments against Set I in 100% of the cases on Map 2 (Fig. 9) and 84% on Map 3 (Fig. 10). The abutting relationships between Sets II and III are mixed, with Set III abutting Set II 26% on Map 2 and 76% on Map 3. Thus, while Set III clearly formed after Set I, formation and propagation of Set II fractures likely continued during or after the formation of Set III.

8. Folding-related fracture subsets

The spatial density of Set III fractures tends to increase with bedding dip. Evidence of this correlation is supported by fracture characteristics at forelimb locations with the greatest dip (>30°). Map 4 (Fig. 13) shows an increase in general fracture density and fracture complexity from fractures mapped at lesser bedding dips (Figs. 8–10). Fracture Sets I, II, and III display chronologically inconsistent abutting relationships, and there are numerous nonsystematic fractures in varying orientations on this Shafer limestone pavement. Two systematic fracture subsets, labeled IV and V, stand out from the nonsystematic fractures because they are more consistently oriented, and occur at multiple locations on the fold where the bedding dip is steepest. The two subsets are not observed to abut or crosscut one another, so their relative ages have not been determined. However, both subsets consistently abut Set III and are interpreted to be younger than Set III.

Fracture abutting relationships suggest a more complex chronology among the major fracture sets in strata with steeper bedding dips (Table 3). On Map 4 (Fig. 13), the number of Set I fractures abutting Set III fractures is roughly equal to the opposite abutting relationship. Also, more Set II fractures abut against Set III fractures than the opposite relationship. These relationships suggest that Set I and Set II fractures reactivated and continued to propagate after the formation of some Set III fractures due to stresses induced during the tilting of the forelimb, or that new fractures in the same orientation as Set I and Set II fractures may have formed by infilling (Bai and Pollard, 2000; Bai et al., 2000; Bergbauer and Pollard, 2004).

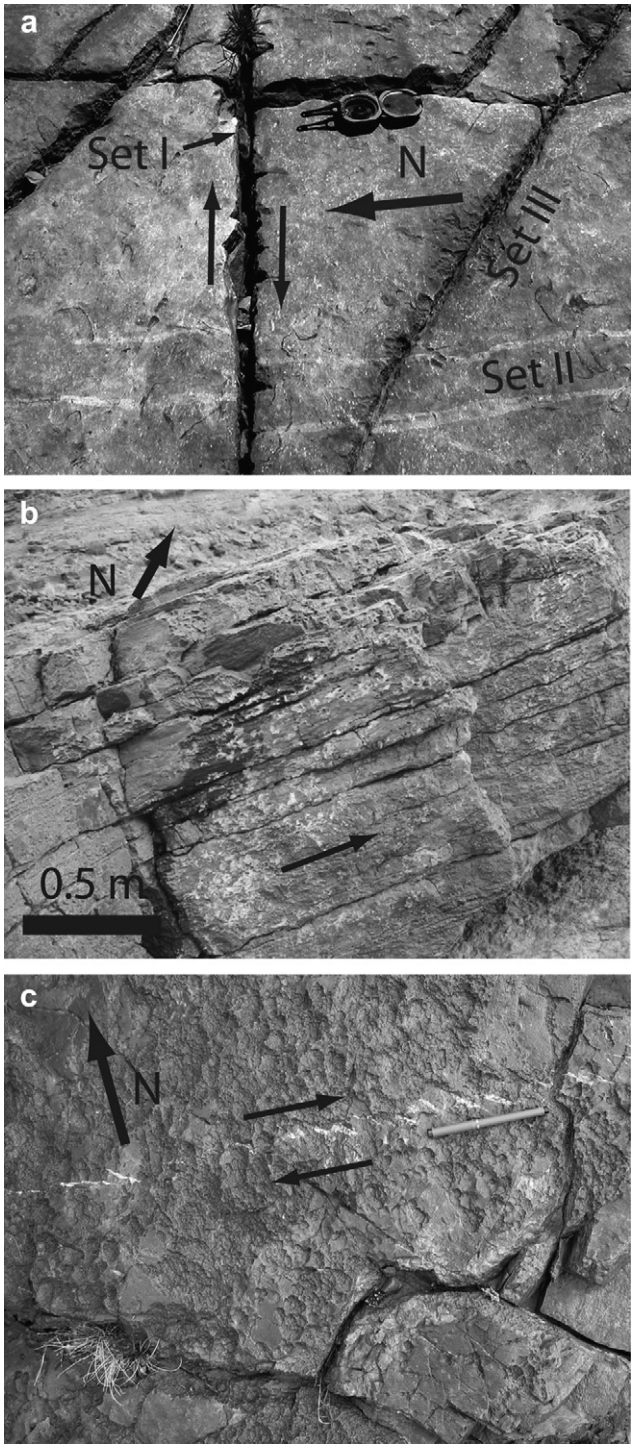

Fig. 11. Evidence of right-lateral slip along Set I fractures in the Unnamed limestone. a) Offset of Set II fractures caused by slip along Set I. Bleaching highlights fracture. View of pavement surface. b) Calcite slickenfibers on a Set I fracture surface. Cross sectional view. c) View of pavement surface with echelon veins. We infer that a Set I fracture is just beneath and perpendicular to this surface with a strike that follows the midpoints of the echelon veins.

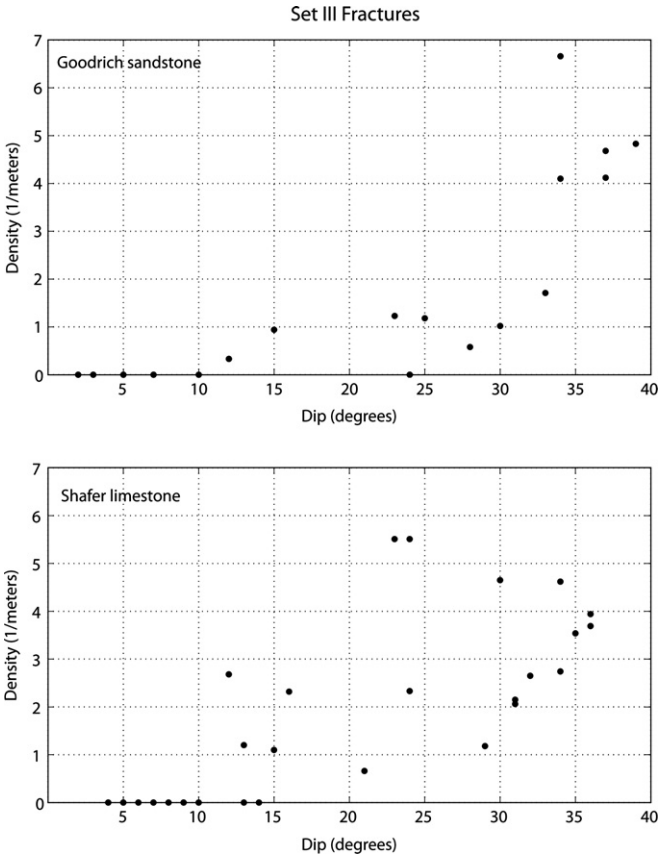

Fig. 12. Plots of Set III density as a function of limb dip for the Goodrich sandstone and Shafer limestone. Density is measured as an average of Set III fractures per meter from three linear 10 m transects measured perpendicularly to Set III strike at each site. Dips are averages of three measurements taken at each site.

9. Conceptual and mechanical models of fracture formation

We present conceptual block models to illustrate the fracture evolution at Raplee Ridge (Fig. 14). These models are composed of three layers, idealized from the stratigraphy of the Rico Formation (Fig. 3), including a red layer representing shale between two grey layers representing sandstone or limestone. The grey layers are erosionally resistant strata which are inferred to be stiffer, that is to have a greater Young's modulus of elasticity (Jaeger et al., 2007), and/or to have a lesser fracture toughness (Anderson, 2005). Stiffer layers carry greater stress than softer layers when subject to the same strain or bending (Timoshenko and Woinowsky-Krieger, 1959). Opening fractures propagate more readily in a less tough layer when subject to the same effective tension (Bai and Pollard, 2000). The grey layers respond to elevated stress during folding by fracturing and by shearing along pre-existing fractures. In contrast, the red layer responds in a more ductile manner, dominantly by plastic flow, resulting in fewer fractures. The interfaces between the brittle and ductile layers may have been bonded, but bedding parallel slip may also have played an important role (Cooke et al., 2000; Couples and Lewis, 2000; Sanz et al., 2007). Arrows, representing the principal stress directions, are presented for three of four block models. Compression is positive and relative magnitudes are $\sigma_1 \geq \sigma_2 \geq \sigma_3$. These would be effective stresses given pore fluid saturation, but we only refer to the orientations and relative magnitudes of the principal stresses.

Fig. 14a shows formation of fracture Set I. During this stage, the strata remained essentially horizontal. The horizontal least compressive stress (σ_3) was oriented almost due N–S and vertical joints formed striking nearly E–W. We note that opening mode fractures constrain only the direction of σ_3. Because σ_1 and σ_2 are restricted to the plane perpendicular to σ_3, the greatest compression could have been vertical, due to the overburden weight. Alternatively, the greatest compression could have been horizontal and nearly E–W, consistent with the Laramide thrusting that

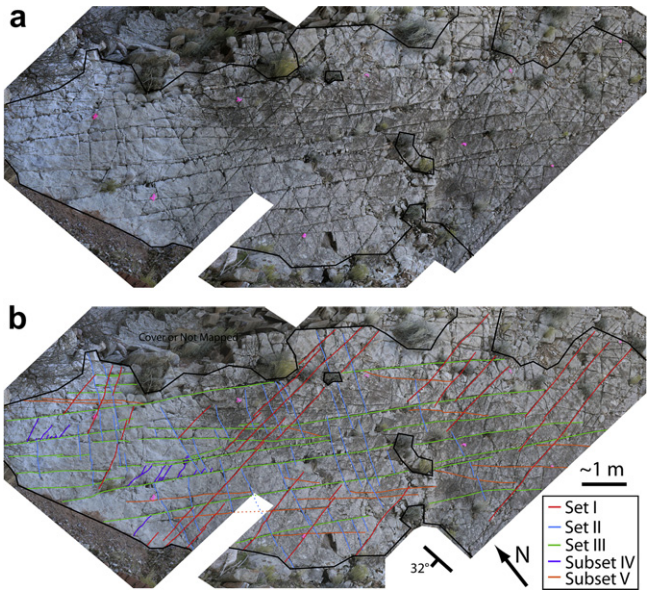

Fig. 13. Fracture Map 4 in the Shafer limestone. The average bedding orientation at this outcrop is ~170°/32°. a) A photograph of the outcrop with an outline of the mapped area. b) Map of Set I, II, and III fractures and Subset IV and V fractures. Many fractures on this outcrop were not mapped because they are not systematic, as defined by Hodgson (1961). Set IV fractures may be interpreted as wing cracks due to left-lateral slip on Set III fractures.

created the much larger Comb Ridge monocline to the east, bounding the Monument Upwarp. In this stage, the stress state was sufficient to cause fracturing across the region mapped by Ziony (Fig. 5), but apparently was insufficient to activate an underlying basement fault at Raplee Ridge.

We infer that Set II fractures formed during a second stress regime some time after Set I and resulted from a local (and perhaps regional) stress state with σ_3 orientated approximately E–W, so that the vertical fractures strike roughly N–S (Fig. 14b). As in Stage 1, the fractures are interpreted as opening mode (joints), based on observed surface textures, which formed before significant folding at Raplee Ridge because they are found on and away from the fold (Fig. 5). Also, both Set I and Set II fractures are perpendicular to bedding both on and off the fold. Set II fractures often are limited to particular mechanical layers, which would be interpreted as having greater Young's moduli and/or lesser fracture toughness, and they are not as consistently oriented as Set I fractures.

A third stage of deformation and a related stress field is shown in Fig. 14c, with the strata tilted about 15° to represent the early period of folding at Raplee Ridge. The conceptual model shows independently forming Set III fractures as well as right lateral shearing of Set I fractures causing the formation of Set III fractures as wing cracks. Temporal association of Set III with the folding, and the possible activation of an underlying thrust fault, is supported by the absence of this set everywhere in the region except on the three folds at Halgaito, Raplee, and Comb Ridges (Ziony, 1966). It is worth noting that the local intermediate compressive stress (σ_2) is inferred to be perpendicular to the bedding and the local greatest compressive stress is ~30° clockwise from Set I,

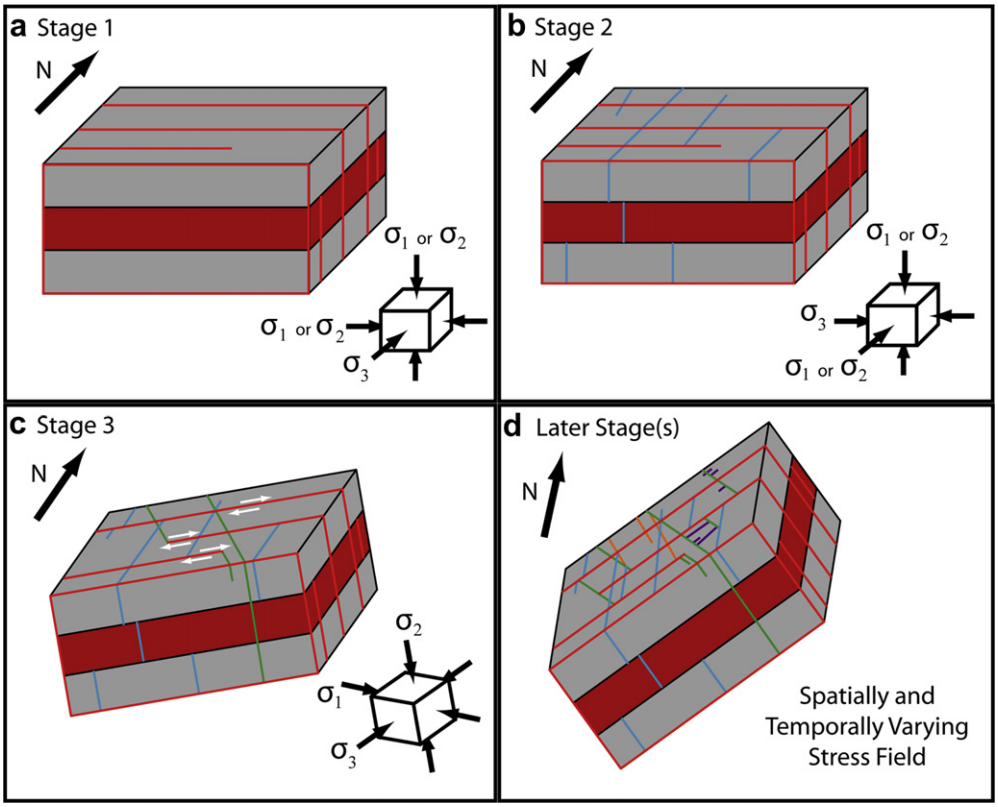

Fig. 14. Conceptual models of deformation stages and fracture formation at Raplee Monocline with inferred orientations and relative magnitudes of local principal stresses. a) Formation of Set I fractures (red) as joints. b) Formation of Set II fractures (blue) as joints. c) Onset of folding leads to tilting of sedimentary layers (10–30°). Set III fractures (green) form from right-lateral shear along Set I fractures and as independently forming joints. d) Continued folding leads to increased bedding dip (>30°). Subsets IV (purple) and V (orange) form and pre-existing fractures infill and continue to propagate.

indicating that the tectonic stress is greater than the overburden stress. It is also interesting to note that the oblique orientation of fracture Set III, relative to the trend of the fold axis, is consistent across the fold.

The conceptual model in Fig. 14d captures many of the structural events that occurred in the later stages of fold growth. As the forelimb dip of the fold increased, presumably due to slip on the underlying thrust fault, fractures in new orientations were created, as evidenced by Subsets IV and V. Additionally, as the dip of the sedimentary layers increased, fractures in Sets I and II reactivated and continued to propagate, often abutting against Set III fractures. This geometry suggests that the compressive stress across Set III fractures was small enough to admit opening or slip of the interface, thereby halting propagation of the reactivated and younger fractures.

The complexity of fracturing during this late deformation stage indicates a spatially and temporally varying stress field. Likely causes for these variations in the local stress state are: 1) pre-existing fractures (Bergbauer and Pollard, 2004); 2) proximity of the forelimb to the upper tip of the thrust fault (Sanz et al., 2007); 3) material heterogeneity, primarily related to differences in mechanical properties of the sandstone, shale, and limestone units within the Rico Formation (Sanz et al., 2008); 4) bedding surface slip (Cooke et al., 2000); and 5) inelastic deformation (Guiton et al., 2003a,b; Casey and Butler, 2004). The complexity of these variations would increase with bedding dip as illustrated in recent model studies (Sanz et al., 2008) and could account for the fracture subsets.

10. Discussion and conclusions

By examining the orientations, abundances, relative ages, and structural relationships of fractures at Raplee Ridge, UT, we identify a fracturing history with distinct stages of occurrence of particular fracture sets and subsets. The proposed multistage evolution of pre- and syn-folding fracture formation includes the reactivation of opening mode fractures (joints) by shearing with the concomitant development of wing fractures, the termination of some propagating fractures against members of older sets, the crossing of other fractures through previously formed fractures, and the infilling of some pre-folding fracture sets on the steepest parts of the fold limb.

Similar to other recent studies of folding-related fractures (e.g. Engelder et al., 1997; Hennings et al., 2000; Bergbauer and Pollard, 2004; Bellahsen et al., 2006; Gross and Eyal, 2007; Olson, 2007), fracture development at Raplee Ridge cannot be explained with conceptual models that suggest relatively simple relationships between structural location on a fold, a local homogeneous stress state, the mode of fracturing (extension versus shear), and fracture orientation (Price, 1966; Stearns, 1969; Cosgrove and Ameen, 2000). The documented field relationships support an interpretation where the stress conditions at particular locations in the fold changed through time, precluding the use of these conceptual models that implicitly require temporal consistency of a stress state at a particular location.

Although we have described sufficient evidence to reject the hypothesis proposed by Ziony (1966) that Set I fractures on Raplee Ridge are composed of two conjugate sets that initiated as shear fractures, we have not rejected this hypothesis for the fractures elsewhere on the Monument Upwarp. Testing that hypothesis using the methodology employed here is a goal of future research.

We have inferred much about the history of fracturing and its relationship to folding at Raplee Ridge from outcrop mapping and orientation data, but additional inferences are likely to come from microscopic observations. For example, petrographic and cathodoluminescence imaging could reveal new information about crack-seal behavior in opening mode fractures and brittle deformation during diagenesis (Milliken and Laubach, 2000; Laubach, 2003; Laubach et al., 2004). Additional work on the petrography of the cements and the fluid inclusions therein could help refine the relative ages of fracturing and fracture reactivation, as well as put constraints on the burial history of the area (e.g. Laubach and Ward, 2006).

Significant differences in fracture characteristics between Raplee Ridge and the surrounding Monument Upwarp, as documented in this study and by Ziony (1966), indicate an important relationship between the folding event and fracturing. We document the presence of a folding-related facture set structurally associated with the forelimb of the fold and mapping by Ziony (1966) suggests this association exists at other folds in the region. The localization of complex fracturing on the forelimb, as well as the fold-oblique orientation of Set III fractures, raises interesting mechanical questions for future investigations about the relationship between fracturing and folding of sedimentary layers, slip between these layers, and possible stresses imposed on those layers by slip along the underlying fault.

Acknowledgements

Thanks to Nicolas Bellahsen, Tricia Fiore, Peter Lovely, Uno Mutlu, Laura Giannone, Danny Zimmerman, Aaron Mynatt, Abby Polus, Barbee Teasley and Jack Mynatt for field assistance. This research was supported by the National Science Foundation's Collaborations in Mathematical Geosciences program, grant number EAR 0417521, and by the Stanford Rock Fracture Project. Reviews by Amy Whitaker, William Dunne, and an anonymous reviewer helped to improve this manuscript.

Appendix. Supporting information

Supplementary data associated with this article can be found in the online version, at doi:10.1016/j.jsg.2009.06.003.

References

Anderson, T.L., 2005. Fracture Mechanics: Fundamentals and Applications, third ed. CRC Press, Boston.
Aydin, A., 2000. Fractures, faults, and hydrocarbon entrapment, migration and flow. Marine and Petroleum Geology 17 (7), 797–814.
Bai, T., Maerten, L., Gross, M.R., Aydin, A., 2002. Orthogonal cross joints: do they imply a regional stress rotation? Journal of Structural Geology 24, 77–88.
Bai, T., Pollard, D.D., 2000. Closely spaced fractures in layered rocks: initiation mechanism and propagation kinematics. Journal of Structural Geology 22, 1409–1425.
Bai, T., Pollard, D.D., Gao, H., 2000. Explanation for fracture spacing in layered materials. Nature 403, 753–756.
Bai, T., Pollard, D.D., 1999. Spacing of fractures in a multilayer at fracture saturation. International Journal of Fracture 100, L23–L28.
Bellahsen, N., Fiore, P., Pollard, D.D., 2006. The role of fractures in the structural interpretation of Sheep Mountain Anticline, Wyoming. Journal of Structural Geology 28, 850–867.
Bergbauer, S., Pollard, D.D., 2004. A new conceptual fold-fracture model including prefolding joints, based on the Emigrant Gap anticline, Wyoming. Geological Society of America Bulletin 116 (3/4), 294–307.
Bergerat, F., Bouroz-Weil, C., Angelier, J., 1992. Paleostresses inferred from macrofractures, Colorado Plateau, western U.S.A. Tectonophysics 206, 219–243.
Bump, A.P., Davis, G.H., 2003. Late Cretaceous-early Tertiay Laramide deformation of the notthern Colotado Plateau, Utah and Colorado. Journal of Structural Geology 25, 421–440.
Bump, A.P., 2003. Reactivation, trishear modeling, and folded basement in Laramide uplifts. GSA Today 13 (3), 4–10.
Casey, M., Butler, R.W.H., 2004. Modelling approaches to understanding fold development: implications for hydrocarbon reservoirs. Marine and Petroleum Geology 21, 933–946.
Cooke, M.L., Moleema, P., Pollard, D.D., Aydin, A., 2000. Interlayer slip and joint localization in East Kaibab Monocline, Utah: field evidence and results from numerical modeling. In: Cosgrove, J.W., Ameen, M.S. (Eds.), Forced Folds and Fractures. Geological Society, London, Special Publication, vol. 169, pp. 23–49.
Cooper, S.P., Goodwin, L.B., Lorenz, J.C., 2006. Fracture and fault patterns associated with basement-cored anticlines: the example of Teapot Dome, Wyoming. AAPG Bulletin 90 (12), 1903–1920.

Cosgrove, J.W., 2000. Forced folds and fractures: an introduction. In: Cosgrove, J.W., Ameen, M.S. (Eds.), Forced Folds and Fractures. Geological Society, London, Special Publication, vol. 169, pp. 1–6.
Cosgrove, J.W., Ameen, M.S., 2000. A comparison of the geometry, spatial organization and fracture patterns associated with forced folds and buckle folds. In: Cosgrove, J.W., Ameen, M.S. (Eds.), Forced Folds and Fractures. Geological Society, London, Special Publication, vol. 169, pp. 7–21.
Couples, G.D., Lewis, H., 2000. Effects of interlayer slip in model forced folds. In: Cosgrove, J.W., Ameen, M.S. (Eds.), Forced Folds and Fractures. Geological Society, London, Special Publication, vol. 169, pp. 129–144.
Coward, M.P., Daltaban, T.S., Johnson, H., 1998. Structural Geology in Reservoir Characterization. In: Fleet, A.J. (Ed.), Geological Society Special Publication. The Geological Society of London, London, vol. 127, p. 266.
Cross, C.W., Spencer, A.C., Purington, C.W., 1899. La Plata Folio. U.S. Geological Survey Atlas Folio GF-0060.
Davis, G.H., 1978. The monocline fold pattern of the Colorado Plateau. In: Matthews, V. (Ed.), Laramide folding associated with basement block faulting in the western U.S.. Geological Society of Americ Memoir, vol. 151, pp. 215–233.
Davis, G.H., 1999. Structural geology of the Colorado Plateau region of southern Utah, with special emphasis on deformation bands. Geological Society of America Special Paper 342, 157 p.
de Joussineau, G., Mutlu, O., Aydin, A., Pollard, D.D., 2007. Characterization of strike-slip fault-splay relationships in sandstone. Journal of Structural Geology 29 (11), 1831–1842.
Delaney, P.T., Pollard, D.D., Ziony, J.I., McKee, E.H., 1986. Field relations between dikes and joints: emplacement processes and paleostress analysis. Journal of Geophysical Research 91 (B5), 4920–4938.
Engelder, T., Gross, M.R., Pinkerton, P., 1997. An analysis of joint development in thick sandstone beds of the Elk Basin Anticline, Montana-Wyoming. Rocky Mountain Association of Geologists Fractured Reservoirs: Characterization and Modeling Guidebook.
Erslev, E.A., 1993. Thrusts, back-thrusts, and detachment of Rock Mountain foreland arches. In: Schmidt, C.J., Chase, R.B., Erslev, E.A. (Eds.), Laramide Basement Deformation in the Rocky Mountain Foreland of the Western United States. Geological Society of America Special Paper, vol. 280, pp. 339–359.
Gilbert, G.K., 1882. On the origin of jointed structure. American Journal of Science 124, 50–53.
Goldstrand, P.M., 1994. Tectonic development of Upper Cretaceous to Eocene strata of southwestern Utah. Geological Society of America Bulletin 106, 145–154.
Gregory, H.E., Moore, R.C., 1931. The Kaiparowits Regions, a geographic and geologic reconnaissance of parts of Utah and Arizona. U.S. Geological Survey Professional Paper, vol. 164.
Griffith, A.A., 1924. The theory of rupture. In: Biezeno, C.B., Burgers, J.M. (Eds.), First International Congress on Applied Mechancis. Delft, J. Waltman, pp. 55–63.
Gross, M.R., Eyal, Y., 2007. Through-going fractures in layered carbonate rocks. Geological Society of America Bulletin 119 (11/12), 1387–1404.
Guiton, M., Leroy, Y., Sassi, W., 2003a. Activation of diffuse discontinuities and folding of the sedimentary layers. Journal of Geophysical Research 108, 2183.
Guiton, M., Sassi, W., Leroy, Y., Gauthier, B., 2003b. Mechanical constraints on the chronology of fracture activation in the folded Devonian sandstone of the western Moroccan Anti-Atlas. Journal of Structural Geology 25, 1317–1330.
Haneberg, W.C., Mosley, P.S., Moore, J.C., Goodwin, L.B., 1999. Faults and subsurface fluid flow in the shallow crust. In: Geophysical Monograph Series, vol. 113. American Geophysical Union, Washington, D.C., pp. 222.
Hennings, P.H., Olson, J.E., Thompson, L.B., 2000. Combining outcrop data and three dimensional structural models to characterize fractured reservoirs: an example from Wyoming. American Association of Petroleum Geologists Bulletin 84, 830–849.
Hilley, G.E., Mynatt, I., Pollard, D.D., 2009. Structural geometry of Raplee Ridge monocline and thrust fault imaged using inverse boundary element modeling and ALSM Data. Journal of Structural Geology, in press.
Hodgson, R.A., 1961. Regional study of jointing in Comb Ridge-Navajo Mountain area, Arizona and Utah. American Association of Petroleum Geologists Bulletin 45, 1–38.
Huntoon, P.W., 1993. Influence of inherited Precambrian baement structure on the localization and form of Laramide monoclines, Grand Canyon, Arizona. In: Schmidt, C.J., Chase, R.B., Erslev, E.A. (Eds.), Laramide Basement Deformation in the Rocky Mountain Foreland of the Western Unisted Stanfes. Geological Society of America Special Paper, vol. 280, pp. 243–256.
Jaeger, J.C., Cook, N.G.W., Zimmerman, R.W., 2007. Fundamentals of Rock Mechanics, fourth ed. Blackwell Publishing, Malden.
Jentgen, R.W., 1977. Pennsylvanian Rocks in the San Juan Basin, New Mexico and Colorado. New Mexico Geological Society Guidebook 28th Field Conference, San Juan Basin III, 129–132.
Jones, G., Fisher, Q.J., Knipe, R.J., 1998. Faulting, Fault Sealing and Fluid Flow in Hydrocarbon Reservoirs. In: Fleet, A.J. (Ed.), Geological Society Special Publications. The Geological Society of London, London, vol. 147, p. 319.
Kelley, V.C., Clinton, N.J., 1960. Fracture systems and tectonic elements of the Colorado Plateau. University of New Mexico, Publications in Geology, no. 6.
Kelley, V.C., 1987. Joints and Fractures. In: Seyfert, C.K. (Ed.), The Encyclopedia of structural geology and plate tectonics. Van Nostrand Reinhold Company Inc., New York, pp. 362–369.
Laubach, S.E., 2003. Practical approaches to identifying sealed and open fractures. American Association of Petroleum Geologists Bulletin 87 (4), 561–579.
Laubach, S.E., Reed, R.M., Olson, J.E., Lander, R.H., Bonnell, L.M., 2004. Coevolution of crack-seal texture and fracture porosity in sedimentary rocks: cathodoluminescence observations of regional fractures. Journal of Structural Geology 26 (11), 967–982.
Laubach, S.E., Ward, M.E., 2006. Diagenesis in porosity evolution of opening-mode fractures, Middle Triassic to Lower Jurassic La Boca Formation, NE Mexico. Tectonophysics 419, 75–97.
Maerten, F., Resor, P., Pollard, D.D., Maerten, L., 2005. Inverting for Slip on Three-Dimensional Fault Surfaces Using Angular Dislocations. Bulletin of the Seismological Society of America 95 (5), 1654–1665.
Maerten, L., Gillespie, P., Daniel, J.M., 2006. Three-dimensional geomechnical modeling for constraint of subseismic fault simulation. American Association of Petroleum Geologists Bulletin 90, 1337–1358.
Miller, C.F., 1955. Photogeologic Map of the Bluff-11 quadrangle, San Juan County, Utah. United States Geological Survey, Miscellaneous Geologic Investigations Map I-54, scale 1:24,000.
Milliken, K.L., Laubach, S.E., 2000. Brittle deformation in sandstone diagenesis as revealed by scanned cathodoluminescence imaging with application to characterization of fractured reservoirs. In: Pagel, M., Barbin, V., Blanc, P., Ohnenstetter (Eds.), Cathodoluminescence in Geosciences. Springer-Verlag, New York, pp. 225–243. Chapter 9.
Murray, G.H.J., 1968. Quantitative fracture study-Spanish pool, McKenzie County, North Dakota. American Association of Petroleum Geologists Bulletin 52 (1), 57–65.
Mutlu, O., Pollard, D.D., 2008. On the patterns of wing cracks along an outcrop scale flaw: A numerical modeling approach using complementarity. Journal of Geophysical Research, 113, B06403, doi: 10.1029/2007JB005284.
Mynatt, I., Hilley, G.E., Pollard, D.D., 2007. Inferring fault characteristics using fold geometry constrained by Airborne Laser Swath Mapping at Raplee Ridge, Utah. Geophysical Research Letters, 34.
Mynatt, I., 2009. Geometric, kinematic and mechanical analyses of faulting, folding and fracturing at Raplee Ridge, UT. PhD Thesis, Stanford University.
National Research Council, Committee on Fracture Characterization and Fluid Flow, 1996. Rock Fractures and Fluid Flow—Contemporary Understanding and Applications. National Academy Press, Washington, D.C.
Olson, J.E., 2007. Fracture aperture, length and pattern geometry development under biaxial loading: a numerical study with applications to natural, cross-jointed systems. In: Lewis, H., Couples, G.D. (Eds.), The Relationship between Damage and Localization. London Geological Society Special Publications, London, vol. 289, pp. 123–142.
Olson, J., Pollard, D.D., 1989. Inferring paleostresses from natural fracture patterns: A new method. Geology 17, 345–348.
O'Sullivan, R.B., 1965. Geology of the Cedar Mesa-Boundary Butte Area, San Juan County, Utah. Geological Survey Bulletin, 1186.
Pollard, D.D., Aydin, A., 1988. Progress in understanding jointing over the past century. Geological Society of America Bulletin 100 (8), 1181–1204.
Price, N., 1966. Fault and Joint Development in Brittle and Semi-Brittle Rock. Pergamon Press, Oxford.
Reches, Z., Johnson, A.M., 1978. Development of monoclines: Part II. Theoretical analysis of monoclines. Geological Society of America Memoir 151, 273–311.
Renshaw, C.E., Pollard, D.D., 1995. The Development of Fracture Connectivity by Propagation Across Unbonded Frictional Interfaces: An Experimentally Verified Criterion. International Journal of Rock Mechanics and Mining Science and Geomechanical Abstracts.
Sanz, P.F., Borja, R.I., Pollard, D.D., 2007. Mechanical aspects of thrust faulting driven by far-field compression and their implications for fold geometry. Acta Geotechnica 2, 17–31.
Sanz, P.F., Pollard, D.D., Allwardt, P.F., Borja, R.I., 2008. Mechanical models of fracture reactivation and slip on bedding surfaces during folding of the asymmetric anticline at Sheep Mountain, Wyoming. Journal of Structural Geology 30, 1177–1191.
Smith, D.A., 1966. Theoretical considerations of sealing and non-sealing faults. American Association of Petroleum Geologists Bulletin 50 (2), 363–374.
Stearns, D.W., 1969. Certain aspects of fracture in naturally deformed rocks. In: Riecker, R.E. (Ed.). Rock Mechanics Seminar. Air Force Cambridge Research Laboratory, Bedford, Mass., pp. 97–118.
Stevenson, G.M., 2000. Geology of Goosenecks State Park, San Juan County, Utah. Utah Geological Association Publication 28, 433–447.
Stone, D.S., 1993. Basement-involved thrust generated folds as seismically imaged in the subsurface of the central Rocky Mountain foreland. In: C.J.S. (Ed.), Larimide basement deformation in the Rocky Mountain Foreland of the Western United States. Geological Society of America Special Publication, vol. 280, pp. 271–312.
Thomas, A.L., 1993. Poly3D: a three-dimensional, polygonal element, displacement discontinuity boundary element computer program with applications to fractures, faults, and cavities in the Earth's crust. Unpublished Ms thesis, Stanford University.
Timoshenko, S., Woinowsky-Krieger, S., 1959. Theory of Plates and Shells. McGraw-Hill Book Company, New York.
Tindall, S.E., Davis, G.H., 1999. Monocline development by oblique-slip fault-propagation folding: the East Kaibab monocline, Colorado Plateau, Utah. Journal of Structural Geology 21, 1303–1320.
Wennberg, O.P., Svana, T., Azizzadeh, M., Aqrawi, A.M.M., Brockbank, P., Lyslo, K.B., Ogilvie, S., 2006. Fracture intensity vs. mechanical stratigraphy in platform top carbonates: the Aquitanian of the Asmari Formation, Khaviz Anticline, Zagros, SW Iran. Petroleum Geoscience 12, 1–11.

Whitaker, A.E., Engelder, T., 2005. Characterizing stress fields in the upper crust using joint orientation distributions. Journal of Structural Geology 27, 1778–1787.
Willemse, E.J.M., Pollard, D.D., 1998. On the orientation and patterns of wing cracks and solution surfaces at the tips of a sliding flaw or fault. Journal of Geophysical Research 103, 2427–2438.
Wu, H., Pollard, D.D., 1995. An experimental study of the relationship between joint spacing and layer thickness. Journal of Structural Geology 17 (6), 887–905.
Ziony, J.I., 1966. Analysis of Systematic Jointing in Part of the Monument Upwarp, Southeastern Utah. Unpublished Ph.D. thesis, University of California in Los Angeles.